In Vitro Biological and Antimicrobial Properties of Chitosan-based Bioceramic Coatings on Zirconium

Salim Levent Aktug
Gebze Technical University
Salih Durdu
Giresun University
Selin Kalkan
Giresun University
Kultigin Cavusoglu
Giresun University
Metin Usta (ustam@gtu.edu.tr)
Gebze Technical University

Research Article

Keywords: Micro arc oxidation (MAO), dip coating, wettability, antibacterial surface, bioactivity, medical applications

Posted Date: February 18th, 2021

DOI: https://doi.org/10.21203/rs.3.rs-208843/v1

Version of Record: A version of this preprint was published at Scientific Reports on July 23rd, 2021. See the published version at https://doi.org/10.1038/s41598-021-94502-z.

Abstract

Ca-based porous and rough bioceramic surfaces were coated on zirconium by micro arc oxidation (MAO). Subsequently, an antibacterial chitosan layer was covered on the MAO-coated zirconium surfaces by dip coating method to develop an antibacterial, bioactive and biocompatible composite biopolymer and bioceramic layer for implant applications. The cubic-ZrO_2, meta-stable $Ca_{0.15}Zr_{0.85}O_{1.85}$, and $Ca_3(PO_4)_2$ were detected on the MAO surface by powder-XRD. The existence of chitosan on the MAO-coated Zr surfaces was verified by FTIR. The micro-pores and thermal cracks on the bioceramic MAO surface were sealed by chitosan coating, while the MAO surface is porous and rough. All elements such as Zr, O, Ca, P and C were homogenously distributed through both surfaces. Moreover, both surfaces indicated hydrophobic properties. However, the contact angle value of the MAO surface was lower than the one of chitosan-based MAO surface. *In vitro* bioactivity on both surfaces was investigated by XRD, SEM and EDX analyses at post-immersion in simulated body fluid (SBF) up to 14 days. *In vitro* bioactivity was significantly enhanced on the chitosan-based MAO surface with respect to the MAO surface. *In vitro* bacterial adhesions on the chitosan-based MAO surfaces were lower compared to the MAO surfaces for *Staphylococcus aureus* and *Escherichia coli*.

1. Introduction

Zirconium that exists in the body only 1 mg on average, does not have a natural biological role in humans [1]. Zirconium can be a potential candidate for surgical implant material due to its promising properties such as low Young's modulus (92 GPa) and excellent biocompatibility compared to titanium and its alloys [2–4]. However, zirconium cannot directly bond to bone tissue at an early stage after implantation due to its bioinert nature [5,6]. In order to overcome this disadvantage, surface treatment enhancing the bioactivity is necessary. The MAO that could form porous, thick, relatively rough and firmly adherent oxide coatings on zirconium surfaces is a promising electrochemical coating technique [2,5,7,8]. However, it is clear that one of the major problems of surface coating techniques is microbial colonization around the implant surfaces whereas their bioactivity and biocompatibility are improved [9–11].

To enhance the anti-microbial property, antibiotics could be presented to the implant surface to reduce the risk of postoperative infection by preventing the microbial adhesion and proliferation [12,13]. However, antibiotic resistance is an important problem requiring primary clinical attention [14]. It is well known that many important pathogens, S. aureus in first line among them exhibit always more alarming levels of antibiotic resistance [15,16]. Furthermore, bacteria forming biofilms on prosthetic surfaces are resistant to antimicrobials [17–19]. Thus, instead of antibiotics, biopolymer chitosan is preferred due to antibacterial properties [20].

The chitosan, which is an important antibacterial agent that has been widely investigated in recent years [21,22]. Chitosan is a natural polysaccharide obtained from by deacetylation of chitin-which is found in exoskeletons of crustaceans and insects, in some fungi and microorganisms [23]. This biopolymer exhibits

excellent features due to nontoxic, biodegradable and promoting cell adhesion. The importance for the antimicrobial properties of chitosan can be explained by the electrostatic interaction between chitosan and bacterial cells [24–26]. Chitosan is a positively charged polymer and protonated amino group of chitosan is appropriate to bind to the negatively charged bacterial cell wall. Moreover, it disrupts the mass transport across the cell wall accelerating the death of bacteria [25,27,28]. Due to this antibacterial property it has been blended with other polymers Therefore, it attach to the DNA to inhibit the replication of bacteria [29]. Thus, a natural biopolymer chitosan is proposed as an important antibacterial agent on the MAO-coated zirconium surfaces in this work.

Some research has been carried out on the fabrication and investigation of properties of chitosan-based MAO surfaces in the literature [21,30–37]. Wang et al. investigated micro RNA-21-loaded chitosan and hyaluronic acid nanoparticles on MAO titanium surfaces [30]. Neupane et al. fabricated chitosan coating on MAO coated Ti surface modified with hydrothermal treatment [31]. Fang et al. investigated immobilization of chitosan film containing semaphorin 3A onto a MAO coated titanium surface via silane reaction to improve MG63 osteogenic differentiation [32]. Cheng et al. made a research on deposition of cefazolin sodium/chitosan composite film on MAO coatings containing Si, Ca and Na on titanium [35]. Li et al. investigated the biological and antibacterial properties of the micro-/nano-structured hydroxyapatite/chitosan coating on titanium [21]. Micro-pores were sealed by the formation of chitosan on the bioceramic MAO-coated titanium and magnesium surface. Usually, the chitosan layer was coated on the MAO coated magnesium and titanium metal surfaces in the literature. However, there is no any study on fabrication and investigation of an antibacterial chitosan-based biopolymer structure on the MAO coated Zr surfaces so far.

In our previous work, antibacterial Ag, Cu and Zn-based nanolayers were produced on the MAO coated Zr surfaces and the biological properties of them were investigated in detail [38–40]. In this work, a natural chitosan-based MAO coatings that were an antibacterial and bioactive were produced on Zr metal at the first time in the literature. Firstly, porous and bioactive Ca-based bioceramic surfaces were coated on Zr metal by the MAO technique. Following the MAO, an antibacterial chitosan layer was uniformly covered onto the MAO surface. The phase structure, functional groups, surface morphology, elemental distribution and hydrophilic/hydrophobic properties of all coatings were analyzed by XRD, FTIR, SEM, EDX-mapping and contact angle measurements, respectively. In addition, *in vitro* predicting bioactivity under body conditions and antibacterial properties for gram-positive (*Staphylococcus aureus*) and gram-negative (*Escherichia coli*) bacteria of both coatings were investigated. Finally, both coatings were compared with each other in detail.

2. Experimental Details

2.1. Sample preparation

The commercial pure zirconium (Zr 702) plates were used as the metal substrates for the MAO process. Initially, the substrates cut into pieces with a size of 30 mm × 25 mm × 5 mm. Then, the substrates were ground by using 400#, 800# and 1200# SiC sandpapers. Finally, they that were cleaned in an acetone in an ultrasonic bath dried under warm air by a heat gun.

2.2. The MAO coating production

In this study, the MAO device (MDO-100WS-100 kW) operated with AC (alternating current) power supply was used as preferred in our previous studies [38–42]. The Zr substrates were served as an anode (working electrode) as stainless steel container was served as a cathode through the MAO process. The MAO electrolyte consisted of 0.25 M calcium acetate and 0.06 M β-calcium glycerophosphate. The electrolyte was prepared by dissolving of all chemicals into de-ionized water [38–42]. The MAO coating productions was carried out at 0.292 A/cm^2 for 10 min. The electrolyte temperature could not exceed 40°C during MAO process by a water-cooling circulator system. After the MAO treatment, they were dried with hot air and preserved in a desiccator.

2.3. Preparation of chitosan solution and coating

The medium molecular weight chitosan used for preparing solutions was purchased from Sigma-Aldrich, Milwaukee. The chitosan was dissolved in 1.0 wt% aqueous acetic acid solution with concentrations of 1.0 vol%. The solutions was stirred for 1 hour until the chitosan completely was dissolved at room temperature. The MAO samples were dipped into the chitosan solution for 5 min. Then, chitosan-coated MAO samples were drawn out at a constant speed and they were dried at 37 °C. This procedure was repeated three times to make sure the solution to cover the micro-pores and thermal cracks of the MAO coating. Finally, to prevent thermal stresses, the chitosan-coated MAO samples were dried in an atmosphere at room temperature for 24 h [36].

2.4. Surface characterization

The phase structures of the MAO coating surfaces was identified by using a powder XRD device (XRD: Bruker D8 Advance) with Cu-Kα radiation at a scanning speed of 1° min^{-1} between 20° and 80°. The chitosan-based MAO coating was probed by using ATR FT IR device (FT IR: JASCO FT/IR 6600) in the wavenumber range from 4000 to 400 cm^{-1}. The discerning of the surface morphologies of both surfaces was observed by using SEM (SEM: Hitachi SU1510). The EDX attached to SEM was used to analyze elemental composition and amounts through both surfaces. The average contact angles were determined by using contact angle goniometer (CAG: Dataphysics OCA 15EC). The CAG device used with a sessile drop technique through all analyses. The average contact angles measurements were carried out within 60 s by using SCA software after the touching of 1 μL distilled water drop onto both coating surfaces.

2.5. Bioactivity properties

In vitro predicting bioactivity of both coatings was evaluated by immersion test in simulated body fluid (SBF). For this experiment, Kokubo and Takadama's SBF recipe (1.0× SBF) was used [43]. Both coatings

were immersed for 14 days in at 36.5°C, with SBF being refreshed every two days. The SBF was prepared by dissolving reagent-grade NaCl, $NaHCO_3$, KCl, $K_2HPO_4{\cdot}3H_2O$, $MgCl_2{\cdot}6H_2O$, $CaCl_2$, and Na_2SO_4 into deionized water and buffering at pH 7.40 with $(CH_2OH)_3CNH_2$ and 1.0 M HCl at 36.5°C. The surface area ratio of the coating surfaces with respect to SBF volume was nearly set equal to 10 [43]. Both coatings were gently washed in distilled water at post-immersion in SBF. Finally, they were spontaneously dried under room temperature and were transferred into desiccators.

At post immersion in SBF, both coatings were analyzed by XRD, SEM, EDX-mapping and EDX-area. The phase structures of both immersed surfaces was investigated by XRD (GNR Europe 600) with Cu-Kα radiation at a scanning speed of 1° min^{-1} from 20° to 80°. The surface morphology of both immersed surfaces was analyzed by SEM (Hitachi SU1510) up to magnification with 10,000×. The elemental distribution and elemental amount on both immersed surfaces were investigated by EDX-mapping and EDX-area analysis.

2.6. Antibacterial properties

Antibacterial properties of the uncoated and chitosan-coated surfaces were determined by agar diffusion test. The antibacterial activity of the surfaces was tested against Gram negative bacteria as *Escherichia coli* ATCC 11293 and a Gram positive bacteria as *Staphylococcus aureus* ATCC 6538. For this purpose, fresh bacterial broth was prepared from stock cultures. Bacterial cultures to be used in agar diffusion test were prepared from the fresh medium of both strains according to McFarland 1.0 standards (10^9 CFU). 100 µL of the prepared suspension was homogeneously spread over the surface of Müller Hinton Agar. The MAO and chitosan-coated MAO surfaces were placed in petri dishes and they were incubated at 37 ° C for 24 hours. The diameter of the inhibition zones (mm) formed around the coating was evaluated for antibacterial properties. Tetracycline and Ceftazidime were used as positive controls for *E. coli* and *S. aureus*, respectively, and all tests were done for three times.

3. Results And Discussion

The phase structure of the MAO coating was investigated by powder XRD analyses as shown in Fig. 1. As seen in XRD spectra, the phases of Zr, cubic-ZrO_2, meta-stable $Ca_{0.15}Zr_{0.85}O_{1.85}$ and $Ca_3(PO_4)_2$ were detected on the MAO surface. Cubic-ZrO_2 and $Ca_3(PO_4)_2$ were observed as major phases, while Zr was found as minor phases in the coating structure. The signal of Zr on XRD spectra derives from the substrate and metallic compounds on the coating. Firstly, the ZrO_2 was formed by the reaction of oppositely charged Zr^{4+} and OH^- ions under high pressure and high temperature on the micro discharge channels at the initial steps of MAO. The instant localized temperature in micro discharge channels reached up to 2500 K through the MAO process as reported in the literature [44]. Therefore, stable cubic-ZrO_2 was observed through whole surface. Moreover, the phase of ZrO_2, which serve as nucleation sites, contributed to the formation of Ca-based phases such as $Ca_3(PO_4)_2$, $Ca_{0.15}Zr_{0.85}O_{1.85}$ and $Ca_{10}(PO_4)_6(OH)_2$ [41,42]. Positively charged Ca^{2+} and negatively charged PO_4^{3-} ions derived from

electrolyte reacted with each other on ZrO_2–based micro discharge channels. And then, $Ca_3(PO_4)_2$ was formed on the MAO surface. Simultaneously, the Zr^{4+} from the substrate and the Ca^{2+} and OH^- from electrolyte combined with each other on micro discharge channels. Then, they form meta-stable $Ca_{0.15}Zr_{0.85}O_{1.85}$ [45].

The FT-IR spectra of the chitosan-based MAO coatings was given in Fig. 2. It designated the characteristic bands of chitosan, ZrO_2 and calcium apatite-based structures. The FTIR peaks located at 560–570, 645–655, 1028, 1089, 1150, 1425, 1590, 1657, 2140–2165, 2340–2380, 2872, 3360–3370 and 3730–3750 cm^{-1} correspond to PO_4^{3-}, OH-, PO_4^{3-}, C-O-C, C-N, N-H, N-H, -NH_2, CO, P-H, C-H, O-H and OH^-, respectively [37,45–53]. Two peaks located at 1089 and 1150 cm^{-1} are characteristic absorption peak of C-O-C and C-N stretching vibration mode, respectively [37,51]. The absorption band peaks at 1425 and 1590 cm^{-1} correspond to N-H band [37,50,51]. The stretching vibration band peak at 1657 cm^{-1} corresponds to $-NH_2$ [37]. The stretching vibration band peaks at 2872 cm^{-1} attributes to C-H in methyl or methenyl [37]. The approximately stretching vibration of non-associated peaks at 3360–3370 cm^{-1} correspond to O-H band [52]. All of these peaks verify the existence of chitosan-based layer structure on the MAO surface [37]. Furthermore, the other peaks support the presence of c-ZrO_2, $Ca_3(PO_4)_2$ and apatite. The characteristic band peak at 1028 cm^{-1} verify to the existence of $Ca_3(PO_4)_2$ [53]. The absorption band peak at 2140–2165 cm^{-1} verify to the existence of c-ZrO_2 [45]. The stretching vibration, libration-deformation, stretching vibration and stretching vibration band peaks at 560–570, 645–655, 2340–2380 and 3730–3750 cm^{-1} verify to the existence of apatite [45–49]. However, crystalline apatite was not observed on the MAO surfaces by XRD as seen in Fig. 1. Thus, it could be concluded that the MAO coatings contained an amorphous apatite structure because it could not kinetically be transformed to crystalline form during MAO process.

The surface morphologies of the MAO and chitosan-based MAO coatings were investigated by SEM as seen in Fig. 3. The surface of the MAO coatings was very porous and rough owing to the presence of micro sparks during the MAO process. Many micropores and voids were found on the MAO surface. The cracks were found on the MAO surface because the thermal stresses appeared between the localized hot surface and cold electrolyte during the process. It is well known that these types of porous and rough bioceramic surfaces are beneficial for cell attachment, proliferation and tissue growth under body conditions for biomedical implant applications. All pores and voids were filled with antibacterial type of chitosan polymer structure after the MAO surface was coated by dip coating method. And then, homogeneous antibacterial chitosan-based MAO surfaces were fabricated on zirconium. After being coated with a chitosan layer on the MAO surface, any micropores, voids and thermal cracks were observed as shown in Fig. 3b. The spherical chitosan structures were monitored on the surface as expected. Thus, it suggests that chitosan-coated MAO surfaces were completely covered.

The elemental distribution found on both surfaces were analyzed by EDX-mapping as illustrated in Fig. 4. The elemental amounts of both surfaces were given in Table 1. As expected, only Ca, P, O and Zr elements

were detected on the MAO surface. The Ca, P and O elements originated in calcium acetate and calcium glycerophosphate-based electrolyte as Zr came from the metallic substrate as expected. Furthermore, all detected elements homogenously distributed through whole the MAO surface were shown in Fig. 4a. Besides the existence of Ca, P and O elements, C was detected on the chitosan-based MAO surface. This element was uniformly dispersed during the surface at post-coating chitosan layer. The chitosan structures naturally contained the C and O elements. However, no Zr elements were observed on the chitosan-based MAO surface. It is concluded that Zr-based oxide structures were found inner layer and the outer surface mainly consisting of Ca-based bioactive and biocompatible elements and phase structures. This situation clearly supported the contribution of ZrO_2 on the formation of Ca-based structures.

Table 1
EDS spectra results of the MAO and chitosan-based MAO coatings

Elements	MAO coating		Chitosan-based MAO coating	
	Wt. %	At. %	Wt. %	At. %
Zr	23.72	6.81	-	-
O	42.14	69.04	49.03	46.36
Ca	24.68	16.14	8.09	3.05
P	9.46	8.00	4.29	2.09
C	-	-	38.45	48.42

The wettability of both surfaces was investigated by a sessile drop - contact angle measurement technique as shown in Fig. 5. The average contact angle values of the MAO and chitosan-based MAO surfaces were measured as 94.0° ± 0.3 and 113.5° ± 0.2, respectively. All measurements were repeated for three times to get an average value of the wettability of the surfaces. Both surfaces had hydrophobic properties since the average contact angle values were bigger than 90°. However, in terms of compassion, the chitosan-based MAO surface indicated hydrophobic character with respect to the MAO surface. The wettability mainly depends on morphological structures/chemical compositions of the surfaces. The MAO surfaces which had many voids and thermal cracks were porous structure as observed in Fig. 3a. The MAO surfaces usually exhibit hydrophilic properties owing to the capillary effect on the liquid of pores [54]. Thus, the water molecules droplet on the MAO surfaces was easily absorbed and spread compared to homogenous chitosan-based biopolymer surface. The highest initial contact angle value was in agreement for the chitosan-coated substrate as reported in the literature and this can be attributed to the basis of its chemical properties [55]. Observed large initial contact angle value can indicate the reorganization of the molecule which is presumably associated with the methyl moieties of the residual acetyl groups along the polysaccharide backbone [56]. Therefore, the wettability of chitosan-based MAO surface was lower than the one of the MAO surface.

In vitro immersion test of the MAO and chitosan-based MAO surfaces were carried out under 36.5 °C in SBF for 14 days. It is well known that this test gives an information about predicting bioactivity of both surfaces. At-post immersion in SBF, the phase structure, surface morphology and elemental distribution of both surfaces were analyzed by XRD (Fig. 6), SEM (Fig. 7) and EDX-mapping (Fig. 8), respectively. Moreover, the amount of the elements formed on both surfaces at post-immersion in SBF was given in Table 2. As seen in Fig. 6, a TCP ($Ca_3(PO_4)_2$) and hydroxyapatite ($Ca_5(PO_4)_3(OH)$)structure was detected as major phase on both surfaces. The Ca^{2+} ions, which released from proteins, adsorb PO_4^{3-} ions by electrostatic interactions in SBF solution [57]. Simultaneously, they react with each other and form $Ca_3(PO_4)_2$ at early stages of immersion in SBF. And then, they react with OH^- ions and transform to $Ca_5(PO_4)_3(OH)$ through the immersion process. The formation mechanism of hydroxyapatite structure occurred on different types such as un-doped and an antibacterial Ag, Cu and Zn-doped MAO surfaces at post-immersion in SBF were discussed in detail in our previous studies [38–42]. The SBF immersion test revealed that chitosan layer was favorable for hydroxyapatite formation. The bioactivity of chitosan was originated due to a large number of protonated amino groups on chitosan surface. Chitosan' surface can absorb OH^- ions in SBF via hydrogen bond and electrostatic attraction. Eventually, they would be adsorbed the Ca^{2+} and PO_4^{3-} in solution by electrostatic attraction. Finally, the reaction of them under SBF conditions form the bone-like apatite on chitosan-based MAO surface [21]. Furthermore, the chitosan layer contribute to nucleate hydroxyapatite because it contains a large amount of OH [58]. It was observed that the amount of crystalline apatite structure formed on chitosan-based MAO surface was greater than the one on the MAO surface as shown in Fig. 6. The original porous bioceramic MAO and spherical biopolymeric chitosan-based MAO surfaces were filled with a new layer at post immersion in SBF. As shown in Fig. 7, a new apatite layer was completely deposited on both surface layer, whereas the chitosan-based MAO surface was nonporous and had polymer structure with respect to the MAO surface. The Ca, P and O are necessary basic elements for the formation of apatite. Only, Ca, P and O elements on both surfaces were observed at post immersion in SBF. Furthermore, all of these were uniformly distributed through the whole surface as shown in Fig. 8. Furthermore, the elemental amount of both surfaces at post-immersion in SBF are the similar as given in Table 2. However, it is clear that a new apatite layer on the chitosan-based MAO surface seem as crack-free and homogenous than the MAO surface. Therefore, it is stated that a chitosan layer on the MAO surface contributed on the formation of apatite structure and improved the bioactivity.

Table 2
EDS spectra results of the MAO and chitosan-based MAO coatings at post-immersion in SBF

Elements	MAO coating		Chitosan-based MAO coating	
	Wt. %	At. %	Wt. %	At. %
Ca	33.23	18.62	33.32	18.69
P	18.19	13.19	18.18	13.19
O	48.57	68.19	48.49	68.12

The antibacterial activities of MAO and chitosan-coated MAO surfaces were examined by agar diffusion test and the results are given in Fig. 9a-9c. The minimum inhibition zone for both strains was obtained with the MAO surfaces. The MAO surface exhibited 5.5 ± 0.7 and 4.2 ± 0.3 mm inhibition zones against *E. coli* and *S. aureus*, respectively. It was observed that after the chitosan coating of the surface, the inhibition zones obtained against bacteria increased significantly. Chitosan-based MAO surfaces exhibited 21.6 ± 1.3 and 13.7 ± 0.9 mm inhibition zones against *E. coli* and *S. aureus*, respectively. It was determined that chitosan-based MAO surfaces have 74.5% more antibacterial activity against *E. coli* than the MAO surfaces. For *S.aureus*, chitosan-based MAO surfaces exhibited 69.3% more antibacterial activity than the MAO counterparts. This result can be related to the antibacterial properties of chitosan coating. Chitosan is the deacetylation product of the chitin molecule. Chitin is a linear biopolymer formed by the bonding of N-acetyl D-glucosamine units by glyosidic bonds [59]. Chitin is insoluble in many solvents due to the compact structure. The lack of solubility in dilute acid or alkaline solvents, especially in water, limits the chitin usability [60]. In order to increase its solubility and usability, the chitin is subjected to de-acetylation with NaOH and high solubility chitosan is formed. Chitosan is a straight-chain polymer consisting of D-glucosamine and N-acetyl D-glucosamine [61]. It contains more amine groups and is easily soluble in acidic solutions. Chitosan, which is physically, chemically and biologically compatible, is known to have medical activities such as antidiabetic, antimicrobial, antioxidant and antitumor [62]. The antibacterial activity of chitosan is due to its polycationic structure [63]. Positively charged chitosan interacts with the negatively charged components of the bacterial cell causing disruptions in normal cell metabolism [64]. It is reported in the literature that many materials coated with chitosan exhibit different levels of antibacterial properties. Zhang et al. reported that chitosan-TiO_2 composite materials exhibit strong antimicrobial activity against *E. coli*, *S. aureus*, *C. albicans* and *A. niger* [65]. In another study, Munteanu et al. found that chitosan-coated polyethylene surfaces provided a 100% inhibition against *S. enteritidis* after 48 hours of interaction, while providing 96.43% inhibition against *E. coli* [66].

Another important result obtained from the antibacterial test is that chitosan-coated MAO surfaces show higher effect against *E. coli* compared to *S. aureus*. This result shows that in general, the chitosan-coated MAO surface is more effective against gram negative compared to gram positive. It was determined that the antibacterial effectiveness of chitosan-coated MAO surfaces against *E. coli* is 1.58 times more than *S. aureus*. This result can be explained by the differences in the cellular structure of gram positive and gram

negative bacteria. The fact that the gram-negative bacteria surface has more hydrophilic character compared to gram-positive bacteria makes them more susceptible to chitosan [67]. The high hydrophilic property leads to greater interaction with chitosan and large changes in the structure and permeability of the cell membrane. These alterations result in bactericidal effects and bacterial death [68]. Similar studies have demonstrated that chitosan-coated surfaces have a higher inhibitory effect against gram-negative bacteria. Munteanu et al. (2014) examined the inhibitory effect of chitosan-coated films with two Gram-negative bacteria, namely *S. enteritidis* and *E. coli*, and a Gram-positive bacteria, *L. monocytogene*s, and reported high inhibition in gram negatives. Esmaeili et al. reported that chitosan-coated nanoparticles exhibited significant antibacterial effect against gram negative bacteria [69]. As a result, it was determined that chitosan-based MAO surfaces have high antibacterial properties compared to the MAO surfaces and exhibit a broad spectrum activity by affecting both gram negative and gram positive bacteria.

Conclusions

In this work, antibacterial and bioactive chitosan-based MAO biopolymer and bioceramic composite surfaces were fabricated on commercial pure Zr by MAO and dip-coating methods. The chitosan-based MAO surface was observed as nonporous and crack-free by post-fabrication dip coating, while the MAO surface was porous and rough due to the existence of micro sparks during the process. All elements such as C, Zr, Ca, P and O, which contributed to form anti-bacterial, bioactive and biocompatible phases, were homogeneously separated during the surfaces. The chitosan-based MAO surface indicated hydrophobic character with respect to the MAO surface because the chemical composition was changed and the porous surface was eliminated. *In vitro* predicting bioactivity and apatite forming abilities of the chitosan-based MAO surfaces were considerably improved to the plain MAO surfaces. Furthermore, microbial adhesions of the chitosan-based MAO surfaces was less than ones of plain MAO surfaces for *E. coli* and *S. aureus*.

Declarations

Acknowledgement

The authors would like to special thank Prof. Emine Yalcin for helping microbial tests at Giresun University and Mr. Ilhan Irende for running SEM and EDS analyses at ODUMARAL.

References

1. Chen, Q. Z. & Thouas, G. A. Metallic implant biomaterials. *Materials Science & Engineering R-Reports.* **87**, 1–57 https://doi.org/10.1016/j.mser.2014.10.001 (2015).
2. Yan, Y. Y. & Han, Y. Structure and bioactivity of micro-arc oxidized zirconia films. *Surf. Coat. Technol.* **201**, 5692–5695 https://doi.org/10.1016/j.surfcoat.2006.07.058 (2007).

3. Johansson, C. B., Wennerberg, A. & Albrektsson, T. Quantitative Comparison of Screw-Shaped Commercially Pure Titanium and Zirconium Implants in Rabbit Tibia. *Journal of Materials Science-Materials in Medicine.* **5**, 340–344 https://doi.org/10.1007/bf00058959 (1994).
4. Thomsen, P. *et al.* Structure of the interface between rabbit cortical bone and implants of gold, zirconium and titanium. *Journal of Materials Science-Materials in Medicine.* **8**, 653–665 https://doi.org/10.1023/a:1018579605426 (1997).
5. Ha, J. Y. *et al.* Enhancement of calcium phosphate formation on zirconium by micro-arc oxidation and chemical treatments. *Surf. Coat. Technol.* **205**, 4948–4955 https://doi.org/10.1016/j.surfcoat.2011.04.079 (2011).
6. Sharkeev, Y. *et al.* Analyzing the Deformation and Fracture of Bioinert Titanium, Zirconium and Niobium Alloys in Different Structural States by the Use of Infrared Thermography. *Metals.* **8**, https://doi.org/10.3390/met8090703 (2018).
7. Yan, Y. Y., Han, Y., Li, D. C., Huang, J. J. & Lian, Q. Effect of NaAlO2 concentrations on microstructure and corrosion resistance of Al2O3/ZrO2 coatings formed on zirconium by micro-arc oxidation. *Appl. Surf. Sci.* **256**, 6359–6366 https://doi.org/10.1016/j.apsusc.2010.04.017 (2010).
8. Lai, P. *et al.* Effect of micro-arc oxidation on fretting wear behavior of zirconium alloy exposed to high temperature water. *Wear.* **424**, 53–61 https://doi.org/10.1016/j.wear.2019.02.001 (2019).
9. Fidan, S. *et al.* Fabrication of oxide layer on zirconium by micro-arc oxidation: Structural and antimicrobial characteristics. *Materials Science & Engineering C-Materials for Biological Applications.* **71**, 565–569 https://doi.org/10.1016/j.msec.2016.11.035 (2017).
10. Violant, D., Galofre, M., Nart, J. & Teles, R. P. In vitro evaluation of a multispecies oral biofilm on different implant surfaces. *Biomed. Mater.* **9**, https://doi.org/10.1088/1748-6041/9/3/035007 (2014).
11. D'Ercole, S., Piattelli, A., Marzo, G., Scarano, A. & Tripodi, D. Influence of bacterial colonization of the healing screws on peri-implant tissue. *Journal of Dental Sciences.* **8**, 109–114 https://doi.org/10.1016/j.jds.2012.12.012 (2013).
12. Asadi, A., Razavi, S., Talebi, M. & Gholami, M. A review on anti-adhesion therapies of bacterial diseases. *Infection.* **47**, 13–23 https://doi.org/10.1007/s15010-018-1222-5 (2019).
13. Gristina, A. G., Hobgood, C. D., Webb, L. X. & Myrvik, Q. N. Adhesive colonization of biomaterials and antibiotic resistance. *Biomaterials.* **8**, 423–426 https://doi.org/10.1016/0142-9612(87)90077-9 (1987).
14. Campoccia, D., Montanaro, L. & Arciola, C. R. The significance of infection related to orthopedic devices and issues of antibiotic resistance. *Biomaterials.* **27**, 2331–2339 https://doi.org/10.1016/j.biomaterials.2005.11.044 (2006).
15. Struelens, M. J. O. D. Methicillin resistant Staphylococcus aureus: toward a coordinated response to a continuing challenge. *Euro Surveill.* **5**, 25–26 (2000).
16. Gold, H. S. & Moellering, R. C. Drug therapy - Antimicrobial-drug resistance. *New England Journal of Medicine.* **335**, 1445–1453 https://doi.org/10.1056/nejm199611073351907 (1996).

17. Mah, T. F. & O., G. A. T. Related articles, mechanisms of biofilm resistance to antimicrobial agents. *Trends Microbiol.* **9**, 34–39 (2001).
18. Schwank, S., Rajacic, Z., Zimmerli, W. & Blaser, J. Impact of bacterial biofilm formation on in vitro and in vivo activities of antibiotics. *Antimicrobial Agents and Chemotherapy.* **42**, 895–898 https://doi.org/10.1128/aac.42.4.895 (1998).
19. Konig, C., Schwank, S. & Blaser, J. Factors compromising antibiotic activity against biofilms of Staphylococcus epidermidis. *European Journal of Clinical Microbiology & Infectious Diseases.* **20**, 20–26 (2001).
20. Battocchio, C. *et al.* Chitosan functionalization of titanium and Ti6Al4V alloy with chloroacetic acid as linker agent. *Materials Science & Engineering C-Materials for Biological Applications.* **99**, 1133–1140 https://doi.org/10.1016/j.msec.2019.02.052 (2019).
21. Li, B. *et al.* Biological and antibacterial properties of the micro-nanostructured hydroxyapatite/chitosan coating on titanium. *Sci. Rep.* **9**, https://doi.org/10.1038/s41598-019-49941-0 (2019).
22. Cremar, L. *et al.* Development of antimicrobial chitosan based nanofiber dressings for wound healing applications. *Nanomedicine Journal.* **5**, 6–14 https://doi.org/10.22038/nmj.2018.05.002 (2018).
23. Santos, V. P. *et al.* Seafood Waste as Attractive Source of Chitin and Chitosan Production and Their Applications. *International Journal of Molecular Sciences.* **21**, https://doi.org/10.3390/ijms21124290 (2020).
24. Li, J. H. & Zhuang, S. L. Antibacterial activity of chitosan and its derivatives and their interaction mechanism with bacteria: Current state and perspectives. *Eur. Polymer J.* **138**, https://doi.org/10.1016/j.eurpolymj.2020.109984 (2020).
25. Liu, H., Du, Y. M., Wang, X. H. & Sun, L. P. Chitosan kills bacteria through cell membrane damage. *International Journal of Food Microbiology.* **95**, 147–155 https://doi.org/10.1016/j.ijfoodmicro.2004.01.022 (2004).
26. Krajewska, B., Wydro, P. & Janczyk, A. Probing the Modes of Antibacterial Activity of Chitosan. Effects of pH and Molecular Weight on Chitosan Interactions with Membrane Lipids in Langmuir Films. *Biomacromolecules.* **12**, 4144–4152 https://doi.org/10.1021/bm2012295 (2011).
27. Raafat, D., von Bargen, K., Haas, A. & Sahl, H. G. Insights into the mode of action of chitosan as an antibacterial compound. *Applied and Environmental Microbiology.* **74**, 3764–3773 https://doi.org/10.1128/aem.00453-08 (2008).
28. Chung, Y. C. & Chen, C. Y. Antibacterial characteristics and activity of acid-soluble chitosan. *Bioresour. Technol.* **99**, 2806–2814 https://doi.org/10.1016/j.biortech.2007.06.044 (2008).
29. Yu, W. Z. *et al.* Synergistic antibacterial activity of multi components in lysozyme/chitosan/silver/hydroxyapatite hybrid coating. *Mater. Design.* **139**, 351–362 https://doi.org/10.1016/j.matdes.2017.11.018 (2018).
30. Wang, Z. S. *et al.* Microarc-oxidized titanium surfaces functionalized with microRNA-21-loaded chitosan/hyaluronic acid nanoparticles promote the osteogenic differentiation of human bone

marrow mesenchymal stem cells. *International Journal of Nanomedicine.* **10**, https://doi.org/10.2147/ijn.S94689 (2015).

31. Neupane, M. P., Park, I. S. & Lee, M. H. Surface characterization and corrosion behavior of micro-arc oxidized Ti surface modified with hydrothermal treatment and chitosan coating. *Thin Solid Films.* **550**, 268–271 (2014).
32. Fang, K. X. *et al.* Immobilization of chitosan film containing semaphorin 3A onto a microarc oxidized titanium implant surface via silane reaction to improve MG63 osteogenic differentiation. *International Journal of Nanomedicine.* **9**, 4649–4657 https://doi.org/10.2147/ijn.S68895 (2014).
33. Zhang, J. *et al.* Degradable behavior and bioactivity of micro-arc oxidized AZ91D Mg alloy with calcium phosphate/chitosan composite coating in m-SBF. *Colloids and Surfaces B-Biointerfaces.* **111**, 179–187 https://doi.org/10.1016/j.colsurfb.2013.05.040 (2013).
34. Liu, P., Pan, X., Yang, W. H., Cai, K. Y. & Chen, Y. S. Improved anticorrosion of magnesium alloy via layer-by-layer self-assembly technique combined with micro-arc oxidation. *Mater. Lett.* **75**, 118–121 https://doi.org/10.1016/j.matlet.2012.02.016 (2012).
35. Cheng, S., Wei, D. Q. & Zhou, Y. Structure of microarc oxidized coatings containing Si, Ca and Na on titanium and deposition of cefazolin sodium/chitosan composite film. *Surf. Coat. Technol.* **205**, 3798–3804 https://doi.org/10.1016/j.surfcoat.2011.01.042 (2011).
36. Bai, K. F. *et al.* Fabrication of chitosan/magnesium phosphate composite coating and the in vitro degradation properties of coated magnesium alloy. *Mater. Lett.* **73**, 59–61 https://doi.org/10.1016/j.matlet.2011.12.102 (2012).
37. Yu, C. *et al.* Self-degradation of micro-arc oxidation/chitosan composite coating on Mg-4Li-1Ca alloy. *Surf. Coat. Technol.* **344**, 1–11 https://doi.org/10.1016/j.surfcoat.2018.03.007 (2018).
38. Durdu, S. *et al.* Characterization and in vitro properties of anti-bacterial Ag-based bioceramic coatings formed on zirconium by micro arc oxidation and thermal evaporation. *Surf. Coat. Technol.* **331**, 107–115 https://doi.org/10.1016/j.surfcoat.2017.10.023 (2017).
39. Durdu, S., Aktug, S. L., Aktas, S., Yalcin, E. & Usta, M. Fabrication and in vitro properties of zinc-based superhydrophilic bioceramic coatings on zirconium. *Surf. Coat. Technol.* **344**, 467–478 https://doi.org/10.1016/j.surfcoat.2018.03.062 (2018).
40. Aktug, S. L., Durdu, S., Aktas, S., Yalcin, E. & Usta, M. Characterization and investigation of in vitro properties of antibacterial copper deposited on bioactive ZrO2 coatings on zirconium. *Thin Solid Films.* **681**, 69–77 https://doi.org/10.1016/j.tsf.2019.04.042 (2019).
41. Aktug, S. L., Durdu, S., Yalcin, E., Cavusoglu, K. & Usta, M. Bioactivity and biocompatibility of hydroxyapatite-based bioceramic coatings on zirconium by plasma electrolytic oxidation. *Materials Science & Engineering C-Materials for Biological Applications.* **71**, 1020–1027 https://doi.org/10.1016/j.msec.2016.11.012 (2017).
42. Aktug, S. L., Durdu, S., Yalcin, E., Cavusoglu, K. & Usta, M. In vitro properties of bioceramic coatings produced on zirconium by plasma electrolytic oxidation. *Surf. Coat. Technol.* **324**, 129–139 https://doi.org/10.1016/j.surfcoat.2017.05.069 (2017).

43. Kokubo, T. & Takadama, H. How useful is SBF in predicting in vivo bone bioactivity? *Biomaterials.* **27**, 2907–2915 https://doi.org/10.1016/j.biomaterials.2006.01.017 (2006).
44. Sandhyarani, M., Rameshbabu, N., Venkateswarlu, K. & Krishna, L. R. Fabrication, characterization and in-vitro evaluation of nanostructured zirconia/hydroxyapatite composite film on zirconium. *Surf. Coat. Technol.* **238**, 58–67 https://doi.org/10.1016/j.surfcoat.2013.10.039 (2014).
45. Aktug, S. L., Kutbay, I. & Usta, M. Characterization and formation of bioactive hydroxyapatite coating on commercially pure zirconium by micro arc oxidation. *Journal of Alloys and Compounds.* **695**, 998–1004 https://doi.org/10.1016/j.jallcom.2016.10.217 (2017).
46. Kokubo, T., Kim, H. M. & Kawashita, M. Novel bioactive materials with different mechanical properties. *Biomaterials.* **24**, 2161–2175 https://doi.org/10.1016/s0142-9612(03)00044-9 (2003).
47. Theunissen, G. S. A. M., Winnubst, A. J. A. & Burggraaf, A. J. Effect of dopants on the sintering behaviour and stability of tetragonal zirconia ceramics. *Journal of the European Ceramic Society.* **9**, 251–263 https://doi.org/10.1016/0955-2219(92)90060-Q (1992).
48. Nayak, Y., Rana, R., Pratihar, S. & Bhattacharyya, S. Low-temperature processing of dense hydroxyapatite-zirconia composites. *International Journal of Applied Ceramic Technology.* **5**, 29–36 https://doi.org/10.1111/j.1744-7402.2008.02180.x (2008).
49. Rapacz-Kmita, A., Paluszkiewicz, C., Slosarczyk, A. & Paszkiewicz, Z. FTIR and XRD investigations on the thermal stability of hydroxyapatite during hot pressing and pressureless sintering processes. *Journal of Molecular Structure.* **744**, 653–656 https://doi.org/10.1016/j.molstruc.2004.11.070 (2005).
50. Halada, G. *et al.* (eds) in BiomaterialsVol. 1054 *ACS Symposium Series* (eds A. S. Kulshrestha, A. Mahapatro, & L. A. Henderson) 159–171 (2010).
51. Sun, T., Wu, C. L., Hao, H., Dai, Y. & Li, J. R. Preparation and preservation properties of the chitosan coatings modified with the in situ synthesized nano SiOx. *Food Hydrocoll.* **54**, 130–138 https://doi.org/10.1016/j.foodhyd.2015.09.019 (2016).
52. Wu, C. S., Hsu, Y. C., Liao, H. T. & Cai, Y. X. Antibacterial activity and in vitro evaluation of the biocompatibility of chitosan-based polysaccharide/polyester membranes. *Carbohydr. Polym.* **134**, 438–447 https://doi.org/10.1016/j.carbpol.2015.08.021 (2015).
53. Zhang, Y. *et al.* Preparation of beta-Ca-3(PO4)(2) bioceramic powder from calcium carbonate and phosphoric acid. *Curr. Appl. Phys.* **5**, 531–534 https://doi.org/10.1016/j.cap.2005.01.026 (2005).
54. Zhang, F. *et al.* Preparation of superhydrophobic films on titanium as effective corrosion barriers. *Appl. Surf. Sci.* **257**, 2587–2591 https://doi.org/10.1016/j.apsusc.2010.10.027 (2011).
55. Farris, S. *et al.* Wetting of Biopolymer Coatings: Contact Angle Kinetics and Image Analysis Investigation. *Langmuir.* **27**, 7563–7574 https://doi.org/10.1021/la2017006 (2011).
56. Bangyekan, C., Aht-Ong, D. & Srikulkit, K. Preparation and properties evaluation of chitosan-coated cassava starch films. *Carbohydr. Polym.* **63**, 61–71 https://doi.org/10.1016/j.carbpol.2005.07.032 (2006).

57. Durdu, S., Usta, M. & Berkem, A. S. Bioactive coatings on Ti6Al4V alloy formed by plasma electrolytic oxidation. *Surf. Coat. Technol.* **301**, 85–93 https://doi.org/10.1016/j.surfcoat.2015.07.053 (2016).
58. Bayrak, G. K., Demirtas, T. T. & Gumusderelioglu, M. Microwave-induced biomimetic approach for hydroxyapatite coatings of chitosan scaffolds. *Carbohydr. Polym.* **157**, 803–813 https://doi.org/10.1016/j.carbpol.2016.10.016 (2017).
59. Schiffman, J. D. & Schauer, C. L. Solid state characterization of alpha-chitin from Vanessa cardui Linnaeus wings. *Materials Science & Engineering C-Biomimetic and Supramolecular Systems.* **29**, 1370–1374 https://doi.org/10.1016/j.msec.2008.11.006 (2009).
60. Subhapradha, N. *et al.* Physicochemical characterisation of beta-chitosan from Sepioteuthis lessoniana gladius. *Food Chem.* **141**, 907–913 https://doi.org/10.1016/j.foodchem.2013.03.098 (2013).
61. Lopez-Mata, M. A. *et al.* Physicochemical and Antioxidant Properties of Chitosan Films Incorporated with Cinnamon Oil. *International Journal of Polymer Science* 2015, doi:10.1155/2015/974506 (2015).
62. Bao, H. N. D. T., S. T. & Physicochemical Properties and Antioxidant Activity of Chitin and Chitosan Prepared from Pacific White Shrimp Waste.*International Journal of Carbohydrate Chemistry*,1–6(2015).
63. Raafat, D. & Sahl, H. G. Chitosan and its antimicrobial potential - a critical literature survey. *Microb. Biotechnol.* **2**, 186–201 https://doi.org/10.1111/j.1751-7915.2008.00080.x (2009).
64. Monarul Islam, M. D., Masum, M. S. D. & Mahbub, K. R. In vitro antibacterial activity of shrimp chitosan against Salmonella paratyphiand Staphylococcus aureus. *Journal of Bangladesh Chemical Society.* **24**, 185–190 (2011).
65. Zhang, X. D. *et al.* Preparation of chitosan-TiO2 composite film with efficient antimicrobial activities under visible light for food packaging applications. *Carbohydr. Polym.* **169**, 101–107 https://doi.org/10.1016/j.carbpol.2017.03.073 (2017).
66. Munteanu, B. S. *et al.* Chitosan Coatings Applied to Polyethylene Surface to Obtain Food-Packaging Materials. *Cellulose Chemistry and Technology.* **48**, 565–575 (2014).
67. Chung, Y. C. *et al.* Relationship between antibacterial activity of chitosan and surface characteristics of cell wall. *Acta Pharmacol. Sin.* **25**, 932–936 (2004).
68. Masson, M. *et al.* Antimicrobial activity of piperazine derivatives of chitosan. *Carbohydr. Polym.* **74**, 566–571 https://doi.org/10.1016/j.carbpol.2008.04.010 (2008).
69. Esmaeili, A. & Ghobadianpour, S. Vancomycin loaded superparamagnetic MnFe2O4 nanoparticles coated with PEGylated chitosan to enhance antibacterial activity. *International Journal of Pharmaceutics.* **501**, 326–330 https://doi.org/10.1016/j.ijpharm.2016.02.013 (2016).

Figures

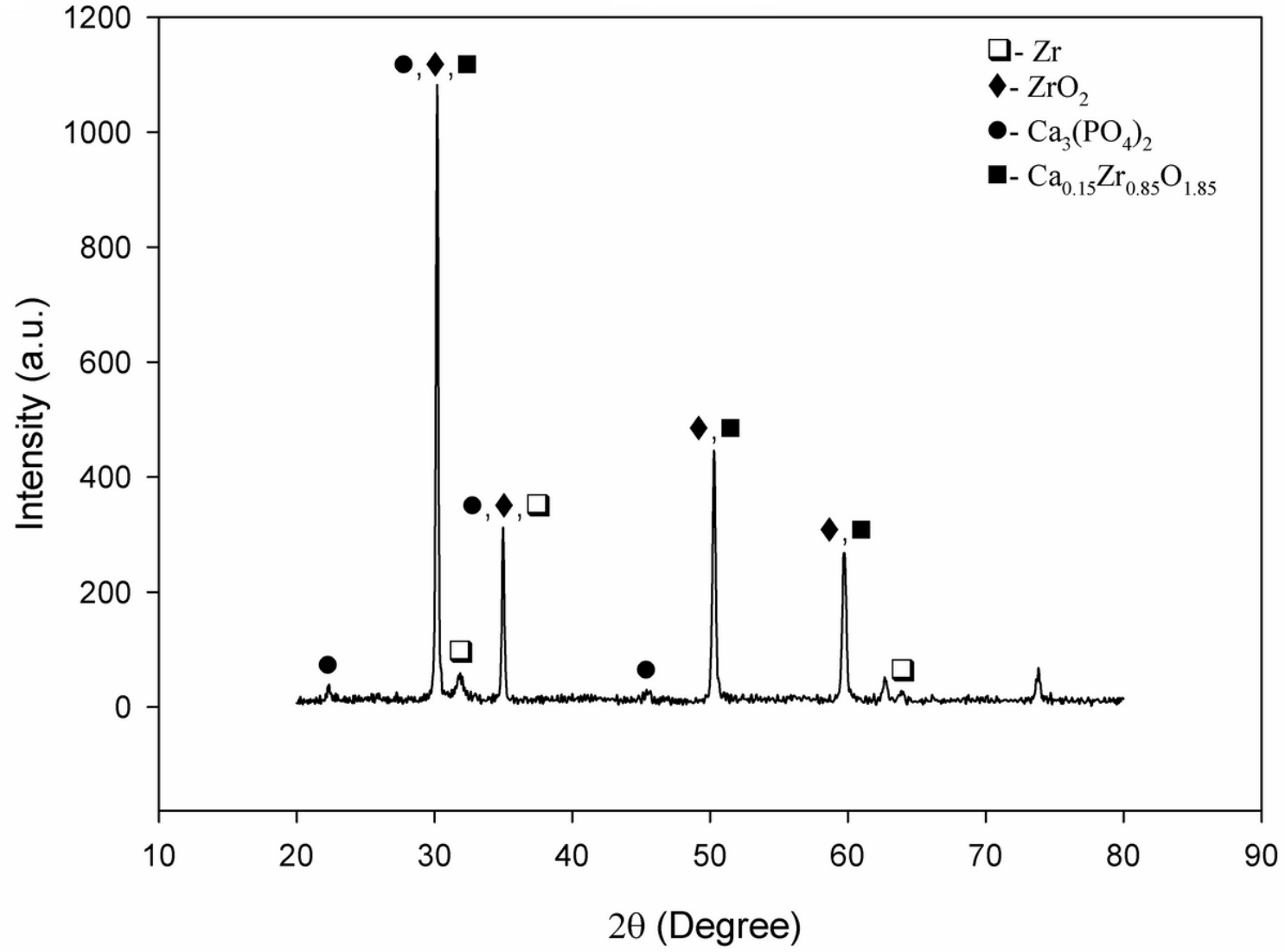

Figure 1

XRD spectra of the MAO coating

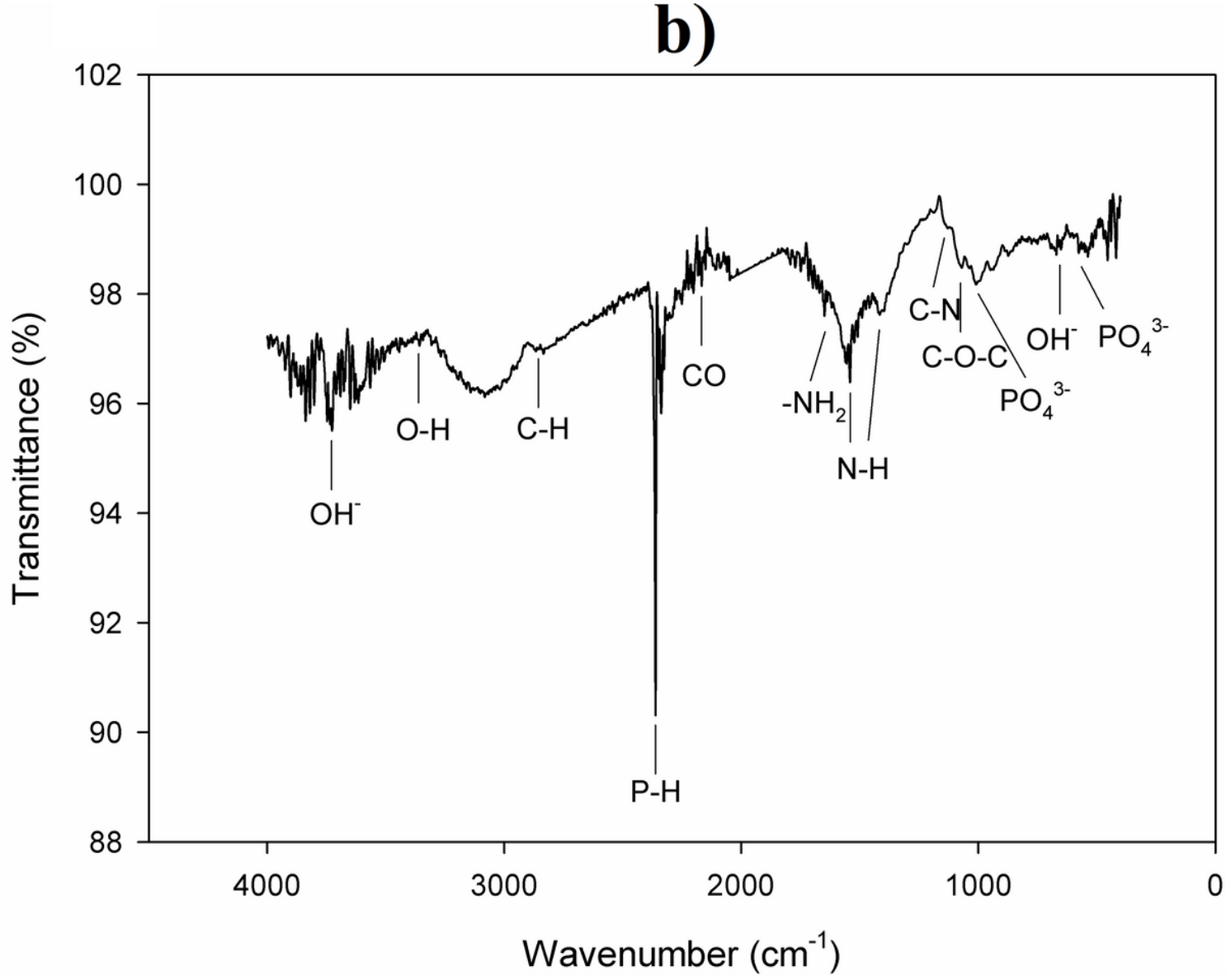

Figure 2

FTIR spectra of the chitosan-based MAO coating

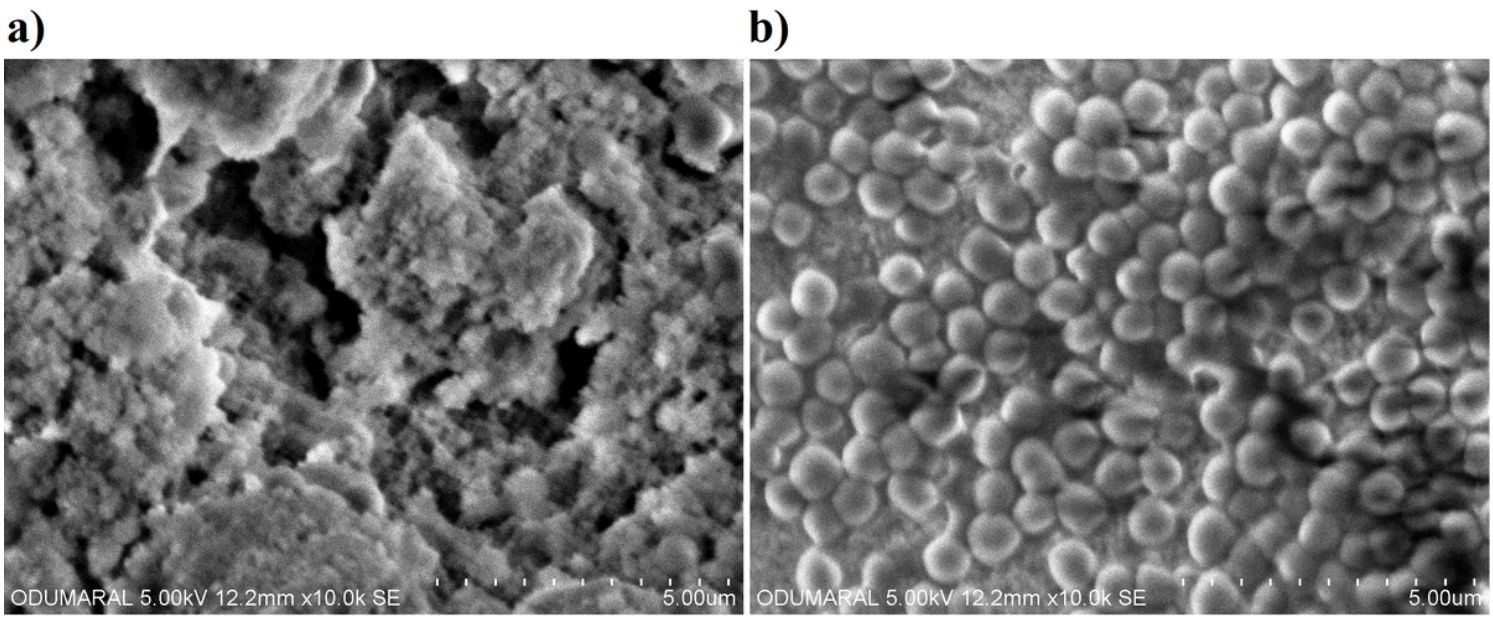

Figure 3

SEM images of the coatings: a) the MAO and b) chitosan-based MAO surfaces

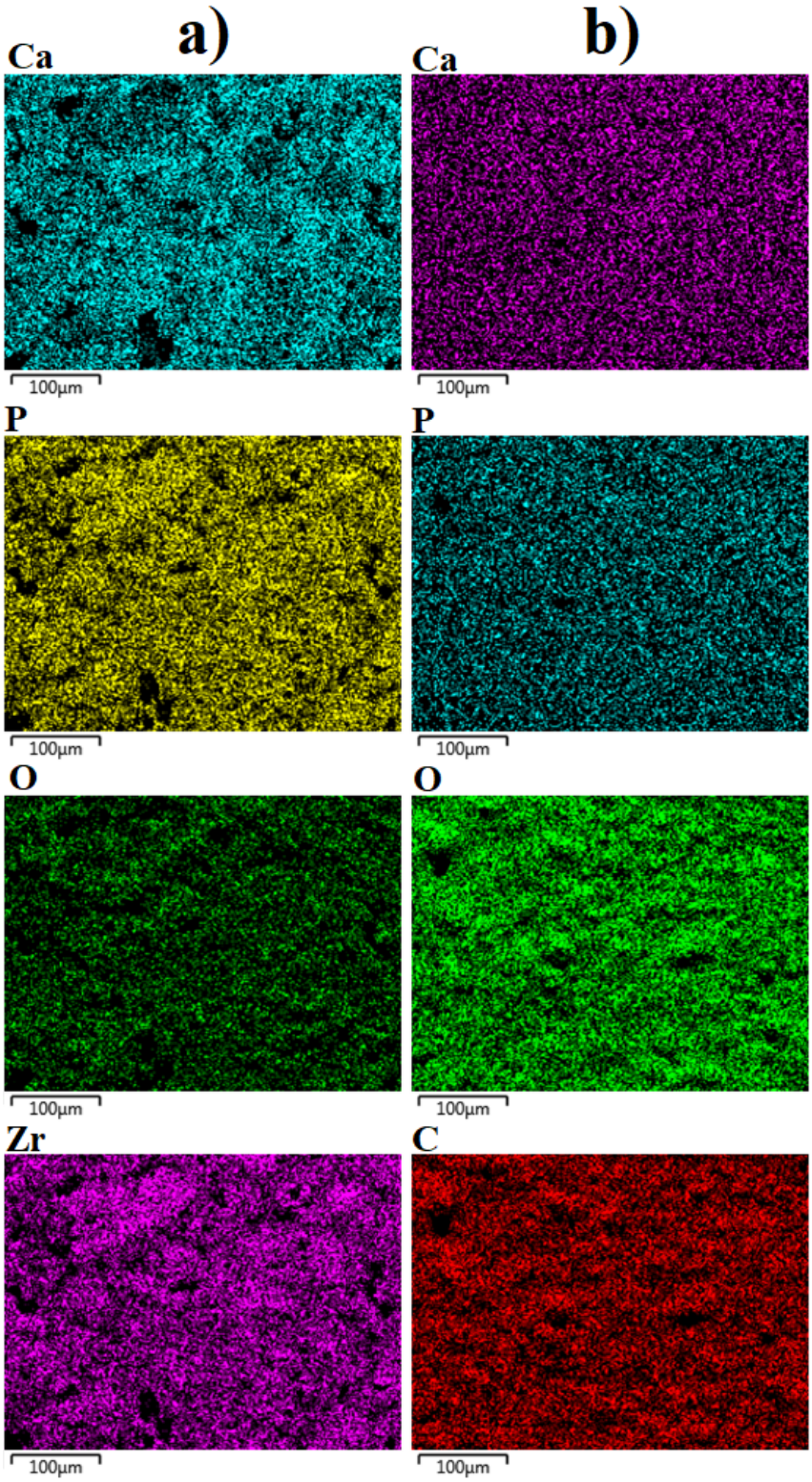

Figure 4

EDX-mapping analysis images of the coatings: a) the MAO and b) chitosan-based MAO surfaces

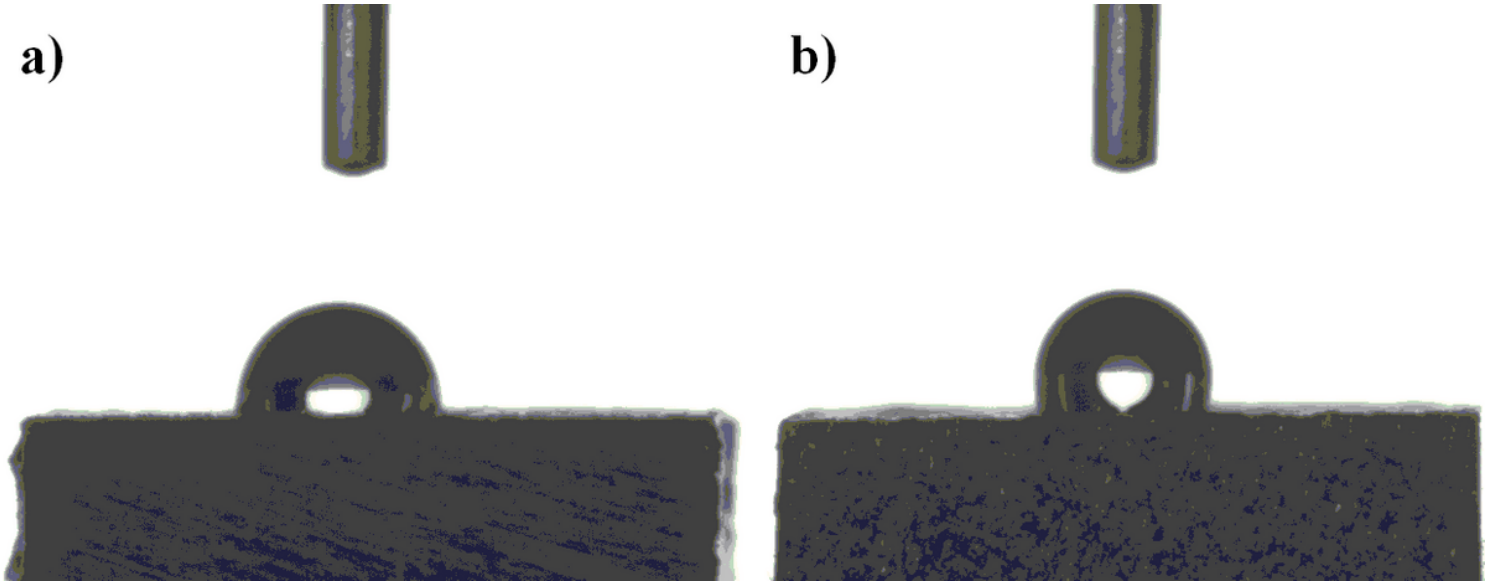

Figure 5

The representative images of droplets contacted on the coatings for 60s a) the MAO and b) chitosan-based MAO surfaces

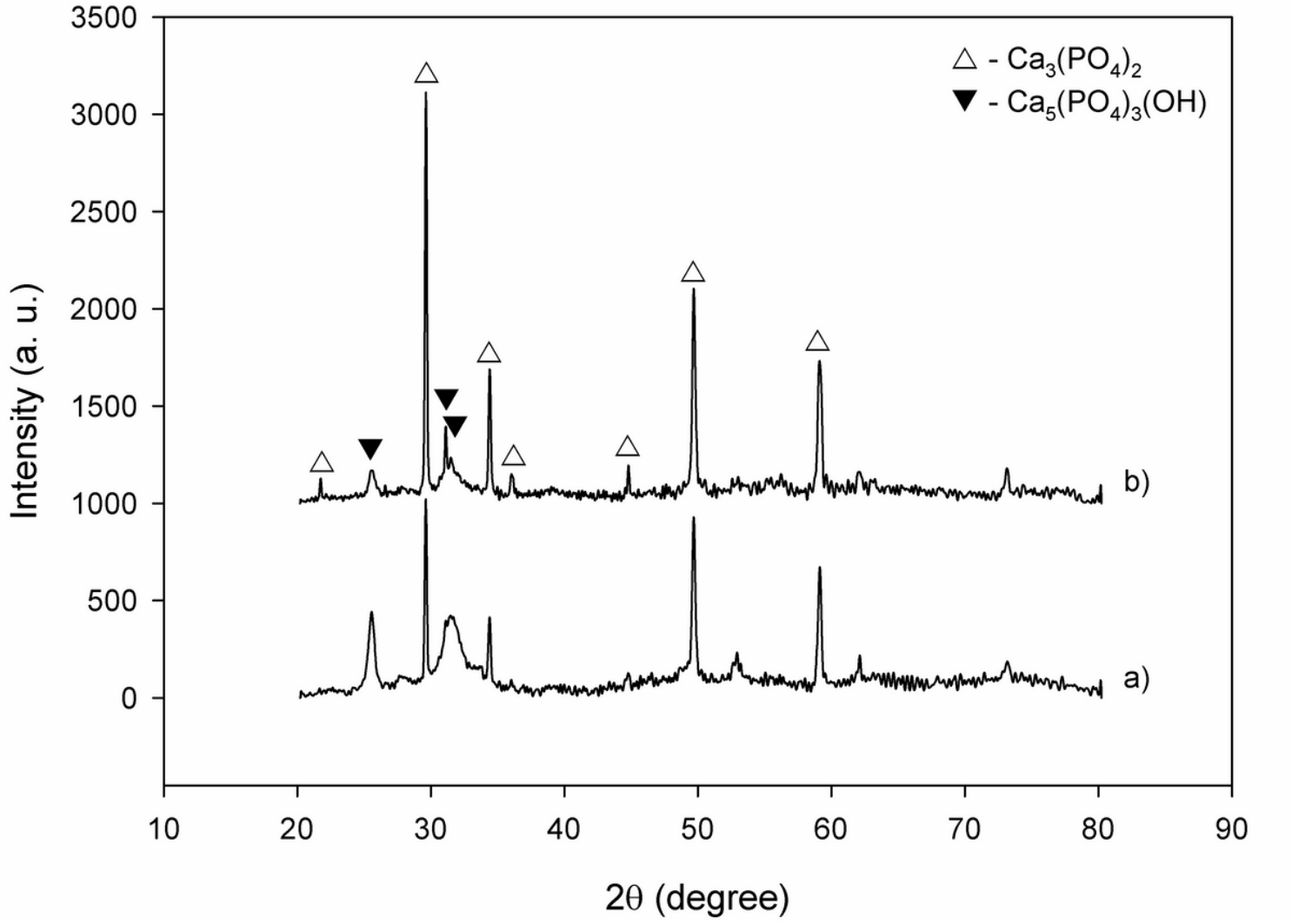

Figure 6

XRD spectra of the coatings at post-immersion in SBF: a) the MAO and b) chitosan-based MAO surfaces

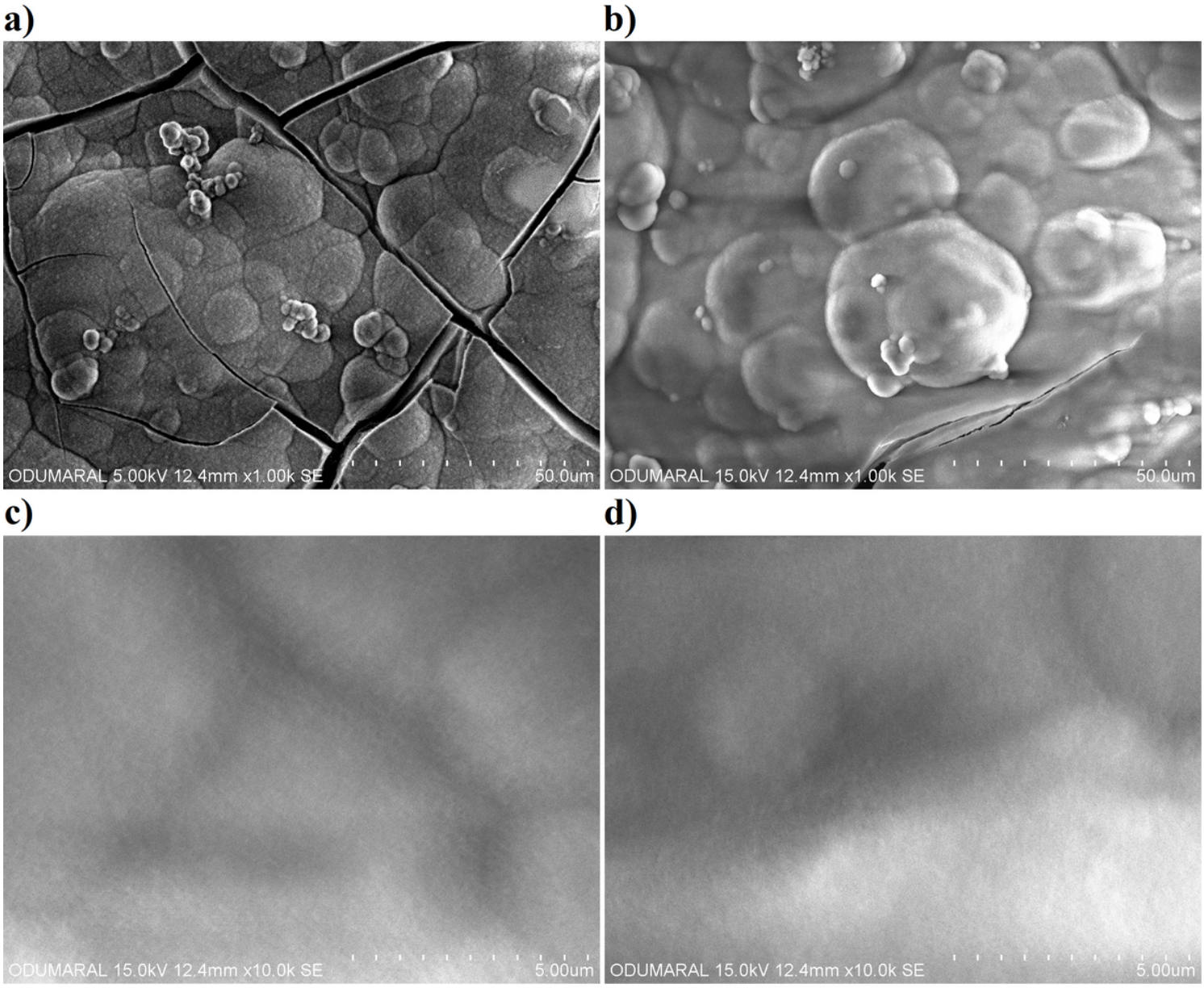

Figure 7

The surface morphologies of the coatings immersed in SBF for 14 days: a) - c) for the MAO and b) - d) for chitosan-based MAO surfaces.

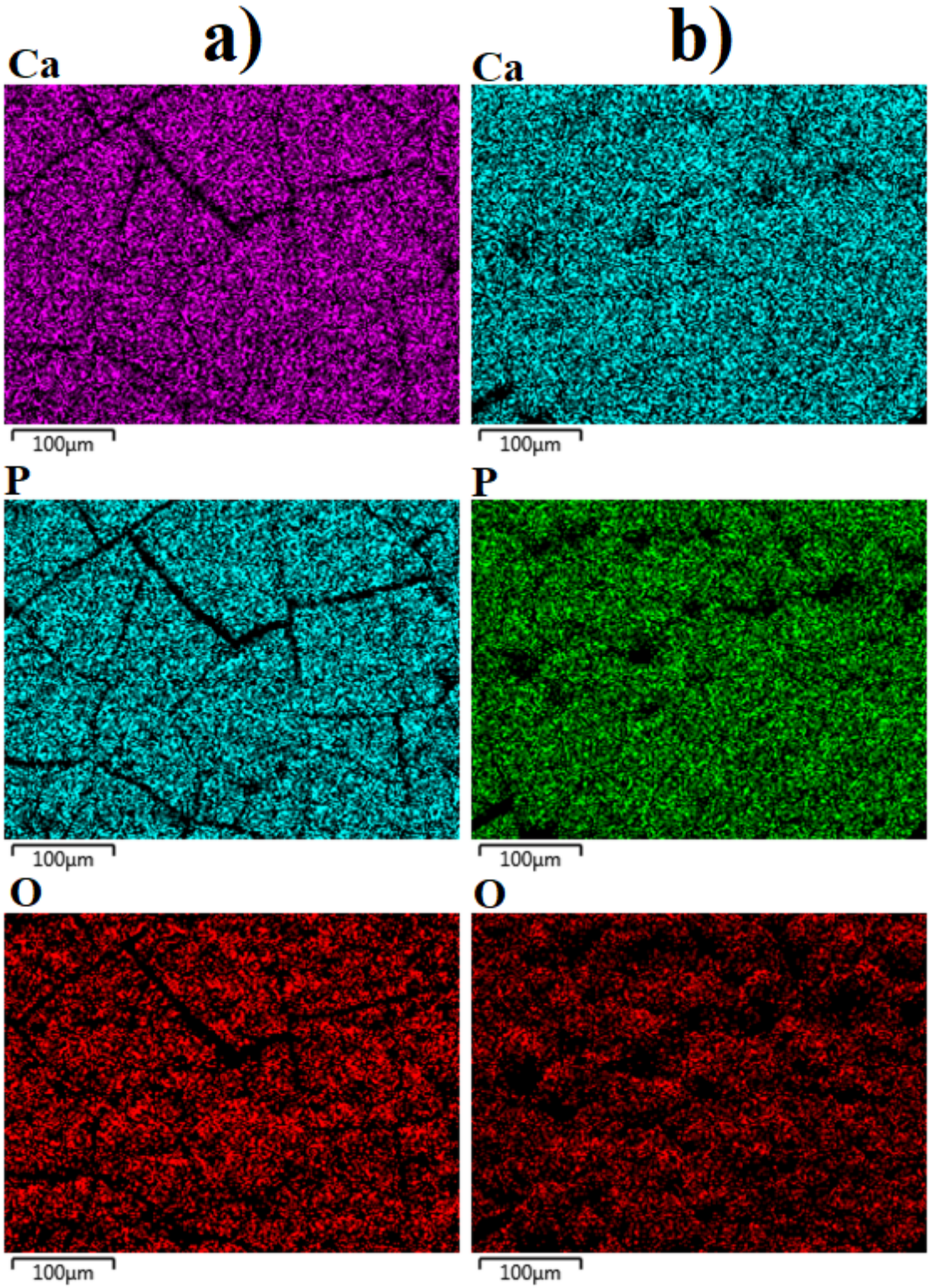

Figure 8

EDX-mapping analysis images of the coatings at post-immersion in SBF: a) the MAO and b) chitosan-based MAO surfaces

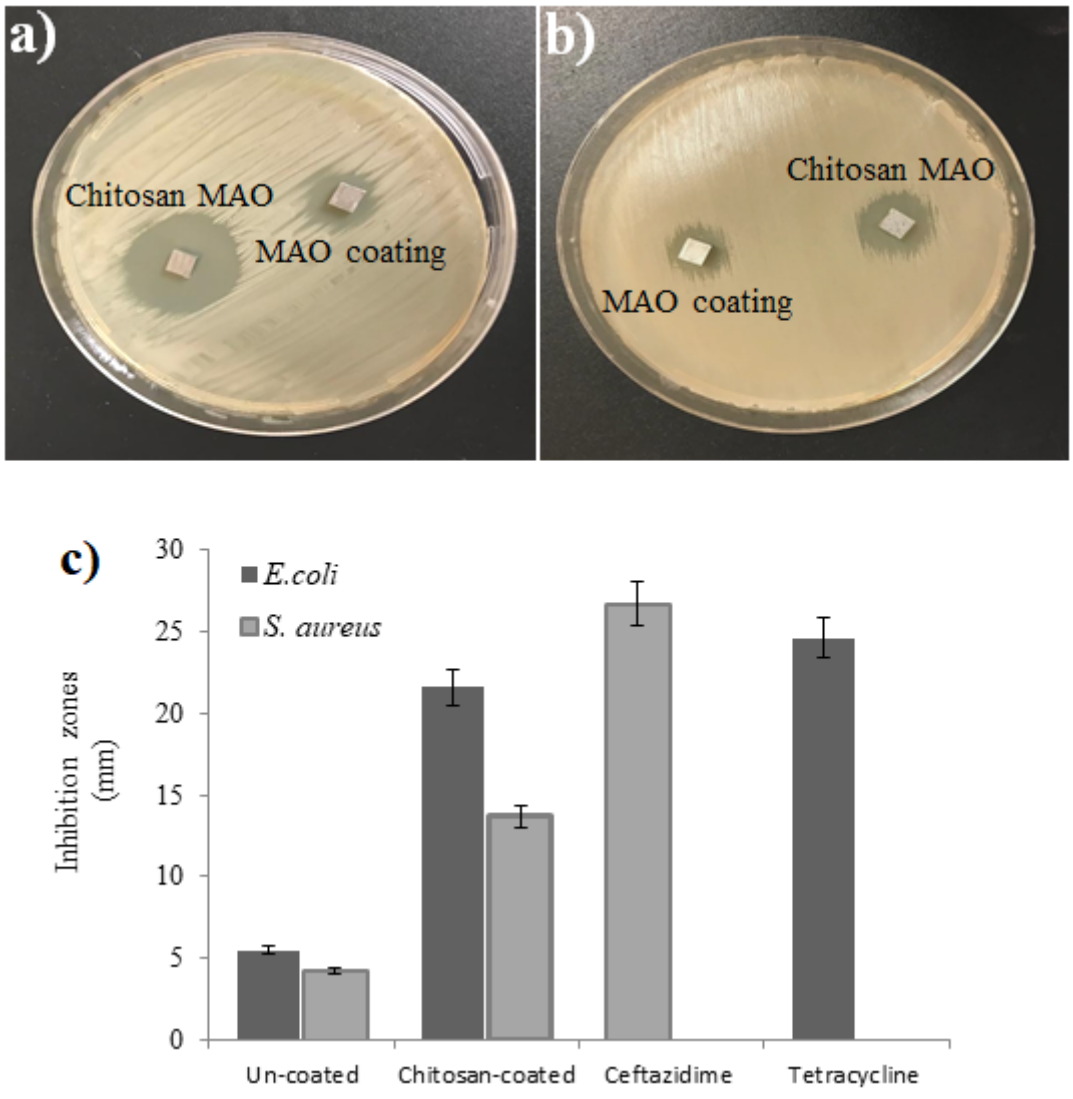

Figure 9

Inhibition zones of the MAO and chitosan-based MAO coated surfaces a) E. coli, and b) S. aureus and c) inhibition zones (mm) of the MAO and chitosan-based MAO surfaces